IEEE Access
Multidisciplinary | Rapid Review | Open Access Journal

Received 9 August 2023, accepted 1 September 2023, date of publication 5 September 2023, date of current version 13 September 2023.

Digital Object Identifier 10.1109/ACCESS.2023.3312058

RESEARCH ARTICLE

Proposed Approach to Investigate the Current and Voltage Distributions of Isolated and Grounded Systems During Earth Fault Conditions

OSAMA E. GOUDA[1], ADEL Z. EL DEIN[2,3], ELSAYED TAG-ELDIN[4], MATTI LEHTONEN[5], AND MOHAMED M. F. DARWISH[6], (Senior Member, IEEE)

[1]Department of Electrical Power Engineering, Faculty of Engineering, Cairo University, Giza 12613, Egypt
[2]Department of Electrical Power Engineering, Faculty of Energy Engineering, Aswan University, Aswan 81528, Egypt
[3]Faculty of Technological Industry and Energy, Thebes Technological University, Luxor 85863, Egypt
[4]Faculty of Engineering and Technology, Future University in Egypt, New Cairo, Cairo 11835, Egypt
[5]Department of Electrical Engineering and Automation, Aalto University, 02150 Espoo, Finland
[6]Department of Electrical Engineering, Faculty of Engineering at Shoubra, Benha University, Cairo 11629, Egypt

Corresponding authors: Osama E. Gouda (prof_ossama11@cu.edu.eg), Mohamed M. F. Darwish (mohamed.darwish@feng.bu.edu.eg), and Matti Lehtonen (matti.lehtonen@aalto.fi)

This work was supported by the Department of Electrical Engineering and Automation, School of Electrical Engineering, Aalto University, Espoo, Finland.

ABSTRACT One important objective of this article is to present a novel approach to study the current density and ground surface potential around the area surrounding earthed and isolated systems in the event of a line-to-earth fault. The present study is done in the case of uniform and two layers of soil. The contact and arc resistances of the line-to-ground faulty conductors are considered. A grounded system is usually implemented with rods and/or grounding grids, the impact of both on step and touch potentials and current density are investigated, discussed, and adapted. The methods of the calculations are based on the electrical concepts, the charge simulation method, and the image method for the grounding system. The results obtained are in agreement with that reported by others, with the benefits of the proposed algorithm for its ease of application, simplicity, and it does not need complex computer programs or a long time in calculations. 3-D dimensions contours of the current density and the electric potential on the earth's surface around the faulty point in case of homogeneous and two layers of soil are presented, whether the network is grounded or isolated. Comparing the results obtained with those reported by the others, differences of 2.2% in the Ground Potential Rise, 2.46% in the current density, and 0.5% in the fault current passes into the isolated system are recorded. These values in the differences are within the acceptable limits.

INDEX TERMS Current and voltage distributions, isolated and grounded systems, earth fault conditions, current density, step and touch potentials.

I. INTRODUCTION

Under fault conditions, a large current flows through the plant structure and equipment into the earth. The research motive in this article is to propose simplified and accurate approaches to study the distribution of step and touch voltages, as well as the distribution of current around the point of contact of the conductor carrying the voltage with the ground in both cases of the isolated and grounded networks, which may cause problems for people near the line to ground faults.

As the grounding resistance is non-zero, the injection of the fault current into the earth produces a ground potential rise (GPR) [1], [2], [3]. That means the electric potential relative to a distant point on the earth's surface is highest at the point where current enters the earth and decays with increasing distance from this point. This ground potential rise can cause hazardous voltage at a distance near and far away from the actual ground fault location depending on the soil resistivity

The associate editor coordinating the review of this manuscript and approving it for publication was Norbert Herencsar.

and the methods of neutral grounding [4], [5], [6]. Many factors affect the level of hazard, such as: the value of the fault current, the ground soil type and its moisture, ambient and ground temperatures, and the clearing time to interrupt the fault [7], [8]. Ground potential rise is an important factor in the design of electrical substations grounding grids, and it is used to determine the safe values of the step, touch, and mesh voltages [4], [8], [9]. Many researchers concur with the calculation of the ground potential rise; no one cares about the calculation of the current density distribution on the ground surface of isolated and grounded systems during earth fault conditions. Based on that, it was necessary to conduct this article. Only Li et al. [10] present a mathematical model for calculating currents along a grounding grid buried in a horizontal multi-layered earth model. This mathematical model was a hybrid of Galerkin's method of moment [11] and the conventional nodal analysis. An electromagnetic model to calculate the distribution of grounding grid potential subjected to lightning surges was presented in references [12], [13]. Current and voltage behavior during a fault in a HV/MV system was investigated in references [14], [15].

The innovations in this article can be summarized as providing new simplified and accurate approaches for the calculations of the distribution of the current density on the earth's surface in case of connecting the faulty conductors with the earth. The cases of isolated and earthed systems in the presence of line-to-ground faults are investigated. The study includes examples of grounding by rods as well as grounding grids. In the present examples, the current density and the electric potential distributions on the ground surface are calculated, as well as the touch and step voltages. The advantages of the proposed approach are its ease of application, simplicity, and it does not need complex computer programs or a long time in calculations.

The paper is organized into seven sections. The first one is the introduction; in addition to the proposed method calculations of the isolated earth and grounded systems, and the governing equations are presented in Sections II and III. Further, Section IV includes the results and discussion of the obtained result and sensitivity analysis of the algorithm to different parameters. The experimental models for the result's validation and the comparison between isolated and grounded systems are presented in Sections V and VI. Finally, Section VII presents the conclusions of the paper.

II. PROPOSED METHOD OF ISOLATED EARTH SYSTEM

In this section, the proposed approaches are discussed for isolated as well as grounded systems.

A. EARTH RESISTANCE OF THE FAULT

With an isolated earth system, the capacitance between the line and the earth gets charged from the supply voltage. During the line to ground fault, the capacitance gets discharged into the earth. Such alternate charging and discharging produce repeated arcs called arcing grounds and the

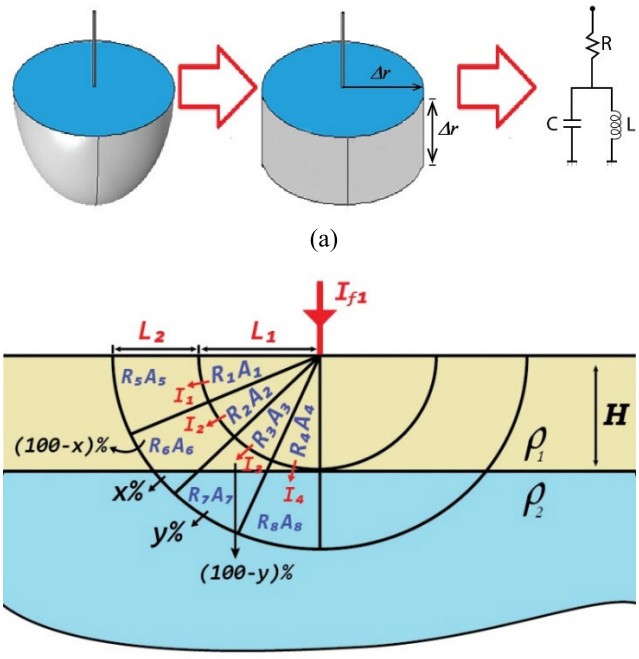

FIGURE 1. Resistance of (a) First shell (hemisphere), and (b) Two-layer soil.

line-to-ground fault current passes through the earth through an arc of air ionization and contact resistance between the arc and the earth at the fault point. The contact resistance, the arc resistance, and the earth resistance damp the line to ground fault current. To calculate the value of the damped fault current it is required to calculate all the mentioned resistances.

The earth resistance of an isolated system in contact with the earth due to line-to-ground fault equals the sum of the resistances of the infinite number of concentric thin hemispheric shells of the soil. In this paper, the resistance of the isolated earth system, in contact with the earth by line-to-ground fault, is calculated, for both homogeneous and two-layer soils, as the sum of the resistances of multi-numbers of concentric thin hemispheric shells of the soil. For a homogeneous soil, the earth is subdivided into an infinite number of concentric thin hemispheric shells of the soil. Actually, the first element (shell) is the hemisphere. To calculate the resistance of this first element, it is assumed to be a cylinder of radius Δr, as well as length equals Δr, as demonstrated in Figure 1(a).

Hence, the resistance of the first cylindrical element is calculated as follows:

$$R_{\Delta r1} = \rho_1 \frac{\Delta r}{\pi \Delta r^2} = \frac{\rho_1}{\pi \Delta r} \tag{1}$$

For other hemispheric shells, the resistance of the shell of number i can be calculated by using equation (2).

$$R_{\Delta ri} = \rho_i \frac{\Delta r}{2\pi r_i^2} \tag{2}$$

The total resistance of the earth is:

$$R_T = R_{\Delta r1} + R_{\Delta r2} + R_{\Delta r3} + R_{\Delta r4} + \dots \quad (3)$$

where ρ_i means the soil resistivity of the shell number i; Δr represents the thickness of each hemispheric shell in the fault current pass and it is assumed to be constant along the fault length; r_i is the radius of the shell of number i; $2\pi r_i^2$ is the area of the hemispheric shell of number i, which represents the cross-section area of the fault current pass. In the case of two layers of soil, each has its own resistivity; the proposed technique should be adapted to consider these two layers. In this case, the soil is divided into two parts; the first one is a hemisphere that has a radius equals the thickness of the first soil layer, and the second is a shell that has a thickness equal to the effective distance minus the thickness of the first soil layer, as shown in Figure 1(b). Each part of these two parts has been divided into four sectors, as shown in Figure 1(b). Each sector has its own resistance, which for sector i can be calculated as follows:

$$R_i = \rho_i \frac{L_i}{A_i} \quad (4)$$

in which ρ_i is the resistivity of the soil of the sector i; L_i is the length of the sector i, which is L_1 for sectors 1, 2, 3, and 4, and L_2 for sectors 5, 6, 7, and 8; and A_i is the area of the sector i, which can be calculated, for the four sectors in Figure 1, as follows: For sectors 1, 2, 3, and 4:

$$A_i = \frac{AA_1}{4} \quad (5)$$

where AA_1 is the average cross-section area of part one (the hemisphere), and is calculated as follows:

$$AA_1 = 2\pi(\frac{L_1}{2})^2 \quad (6)$$

For sectors 5, 6, 7, and 8:

$$A_i = \frac{AA_2}{4} \quad (7)$$

in which AA_2 is the average cross-section area of part two which can be considered as a shell, and it is calculated by using equation (8).

$$AA_2 = 2\pi(L_1 + \frac{L_2}{2})^2 \quad (8)$$

From Figure 1(b), it is noticed that some sectors are located in the two layers, such as sector number six. In this case, its resistance is calculated by using equation (9).

$$R_6 = x.R_8 + (1 - x).R_5 \quad (9)$$

where x is the fraction of sector six that was located in the second layer, which is the same as that of sector number eight, and (1-x) is the fraction of sector six that was located in the first layer, which is the same as that of the sector number five.

To calculate the contact resistance between the faulty conductor and the isolated earth system, Maxwell's formula is used [16], [17]. It is assumed that the faulty conductor of the isolated earth touches the ground surface at a single circular spot of radius a, hence, the formula for the contact resistance is as given in equation (10) [18], [19], [20], [21]:

$$R_{cont} = \frac{\rho}{2a} \quad (10)$$

where ρ means the electrical resistivity of the contact member and a means the contact spot radius. To calculate the contact resistance, the assumptions of the theory of Holm [18] are used. It is assumed that the a-spot has a zero thickness, and the current channel has a resistivity ρ equals the average value of the conductor and the soil resistivity.

B. ARC RESISTANCE

The arc resistance mainly depends on the arc (fault) current, the arc length and air humidity, pressure, and temperature. There are many formulae for the calculation of arc resistance [22], [23]. Each formula was obtained from experiments done with a particular range of currents; however, they have been employed in a wider range. The arc length in this study is assumed to be 20 cm and the arc (fault) current is taken as 1000 A, hence the obtained value of the arc resistance is ranged between 0.17 and 0.3 Ω. The arc resistance is small compared with the values of the contact resistance and the earth resistance of the fault results in a slight effect on the obtained results. In general, the following formula is used to calculate the arc resistance [24], [25].

$$R_{arc} = \frac{27677.5\,L}{I_f^{1.4}} \quad (11)$$

where L means the arc length and I_f called the fault current.

C. DAMPED CURRENT

The contact resistance as well as the arc resistance will damp the fault current I_f by a certain value. The damped fault current I_{f1}, which will pass into the isolated earth, can be estimated by the use of the following relation:

$$I_{f1} = \frac{I_f R_T}{(R_T + R_{cont} + R_{arc})} \quad (12)$$

D. CALCULATION OF FAULT CURRENT DENSITY AND ELECTRIC POTENTIAL IN CASE OF HOMOGENEOUS SOIL

The fault current, I_{f1}, will pass through an infinite number of thin hemispheric shells of the soil, as seen in Figure 1(b). That means the fault current will flow uniformly in all directions through these series of hemispheric shells of the soil. To calculate the surface electric potential distribution in this case, it is required to compute the distribution of the current and the hemispheric shell resistance.

Hence, at any distance r from the faulty point, the fault current density at the earth's surface can be obtained by using relation (13).

$$J = \frac{I_{f1}}{2\pi r^2} \quad (13)$$

Also, for a hemisphere shell of thickness Δr located at distance r from the faulty point, the electric potential difference

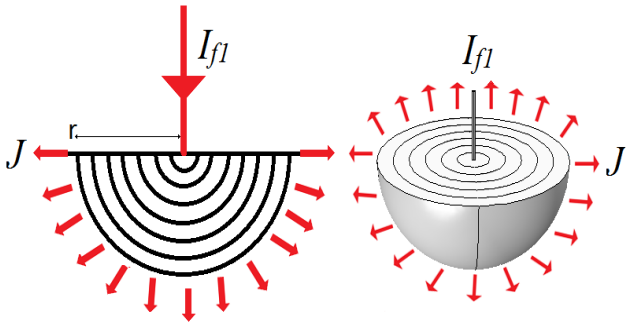

FIGURE 2. Distribution of the fault current in the hemispheric shells of the soil.

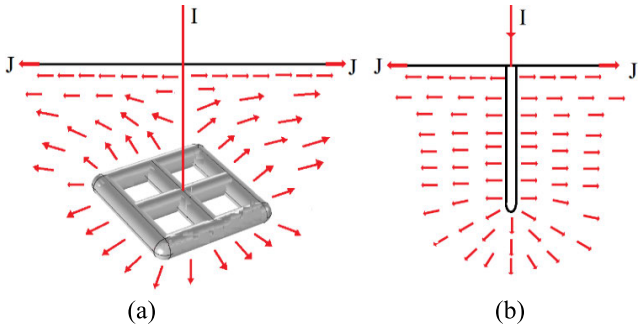

FIGURE 3. Distribution of the fault current inside the earth with grounding system, (a) grid and (b) rod.

across its thickness Δr can be determined as follows:

$$V_{\Delta r} = R_{\Delta r} I_{f1} = \rho \frac{\Delta r I_{f1}}{2\pi r^2} \tag{14}$$

From equations (13) and (14), the distribution of the fault current density and the distribution of the electric potential rise at the earth's surface with respect to a reference point are obtained.

Also, in the case of two layers of soil, the fault current, I_{f1}, will pass through an infinite number of thin hemispheric shells of the soil, as demonstrated in Figure 2.

To calculate the current, I_1, which passes in the nearest sectors to the earth's surface, the following set of equations is developed, considering the outer radius of the second part (the shell) is far away from the fault point and all its points have the same potential with respect the potential of the fault point.

$$I_1 (R_1 + R_5) = I_2 (R_2 + R_6) \tag{15}$$

$$I_1 (R_1 + R_5) = I_3 (R_3 + R_7) \tag{16}$$

$$I_1 (R_1 + R_5) = I_4 (R_4 + R_8) \tag{17}$$

$$I_1 + I_2 + I_3 + I_4 = \frac{1}{2} I_{f1} \tag{18}$$

Hence,

$$I_1 = \frac{1}{2} I_{f1} \left(\frac{1}{k_1 + k_2 + k_3}\right) \tag{19}$$

where,

$$k_1 = \frac{R_1 + R_5}{R_2 + R_6}, \tag{20}$$

$$k_2 = \frac{R_1 + R_5}{R_3 + R_7} \tag{21}$$

and

$$k_3 = \frac{R_1 + R_5}{R_4 + R_8} \tag{22}$$

Once, the current I_1 is calculated, the current density J_1 at any distance r from the fault point on the earth's surface can be obtained as follows:

$$J_{1r} = \frac{n.I_1}{2\pi r^2} \tag{23}$$

where n is the number of sectors as in Figure 1(b) $n = 4$. Also, the potential difference across any thickness Δr can be calculated as follows:

$$V_{\Delta r} = R_{\Delta r} I_1 = \rho_1 \frac{n.\Delta r I_{f1}}{2\pi r^2} \tag{24}$$

Hence, from equations (23) and (24), the distribution of the fault current density and the distribution of the electric potential rise at the earth's surface with respect to a reference point, for a soil of two layers can be obtained. The two cases illustrated in Figure 1 represent the homogeneous soil and the soil consisting of two layers. They are the most common in the design of grounding grids. In the case of multi-layer soils, the soil layers can be reduced to two only by using the apparent soil resistivity as reported by reference [26], (two layers of soil can be combined to form one layer), and then the problem can be solved by the present method. This is one of the negative points of this approach. More examination of this topic will be done in the future.

III. PROPOSED METHOD OF GROUNDED SYSTEM

The grounding systems ensure maximum safety from electrical faults and lightning by grounding system contains rods or grids; there are two probabilities for the fault current to pass into the earth. Firstly, the fault current will pass into the earth during its passing to the ground system, as with the grounding grid given in Figure 2. Secondly, the fault current will pass into the earth from the ground system itself, as with a grounding rod in Figure 3.

Actually, it is difficult to calculate the distribution of the current density in the same way as in the previous section, as the fault current does not flow uniformly into an infinite number of thin hemispheric shells of the soil, especially at a distance relatively near to the grounding system. In this case, for homogeneous soil or two layers of soil, the distribution of the ground potential rise will be calculated by any analytical or numerical method, such as the charge simulation method with the image method [24]. Once the ground potential rise was calculated, the distribution of the current density at the earth's surface can be calculated as follows:

$$J = \frac{V_{\Delta r}}{\rho \Delta r} = \sigma E \tag{25}$$

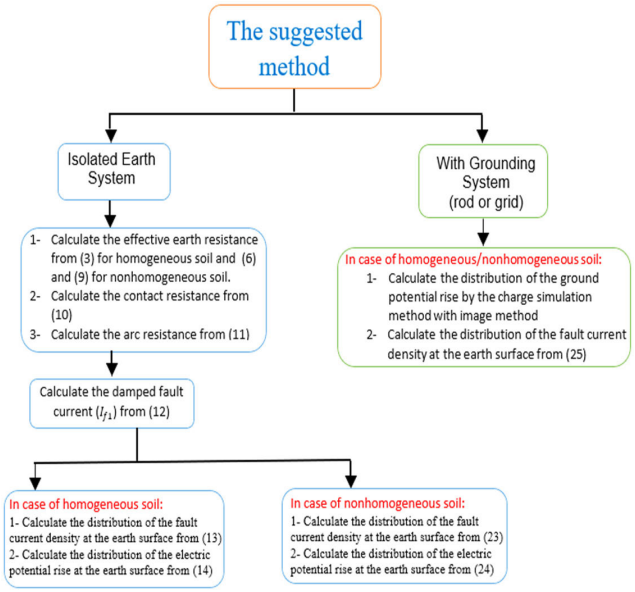

FIGURE 4. Flowchart of the proposed calculations.

In two layers soil, the apparent soil resistivity ρ_a can be computed according to IEEE 80-2013 [27], [28].

$$\rho_a = \frac{\rho_1}{\left[1 + \left[(\frac{\rho_1}{\rho_2}) - 1\right][1 - e^{\frac{1}{k(z+2h)}}]\right]} \quad \text{For } \rho_2 < \rho_1 \quad (26)$$

$$\rho_a = \rho_2 \times [1 + \left[(\frac{\rho_2}{\rho_1}) - 1\right][1 - e^{\frac{-1}{k(z+2h)}}]] \quad \text{For } \rho_2 > \rho_1 \quad (27)$$

where h is the grid depth, k is the reflection factor $k = [(\rho_2 - \rho_1) / (\rho_1 + \rho_2)]$, z is the thickness of the soil top layer, ρ_1 is the resistivity of the upper soil and ρ_2 is the resistivity of lower soil.

IV. RESULTS AND DISCUSSION

The calculations carried out by the proposed method for isolated as well as grounded systems are summarized in the following flowchart given in Figure 4.

A. ISOLATED SYSTEM RESULTS

In the present study, the fault current is taken as 1000 A. The resistivity of the faulty conductor (Aluminum) is considered 2.65×10^{-8} Ω.m, the soil resistivity is supposed to be 100 Ω.m, and hence, the resistivity of the contact member has been considered as the average of the two resistivities. The contact spot radius is taken as the conductor radius of 15 mm. The effective earth resistance obtained from equation 3 is 500 Ω, and the summation of contact and arc resistances according to equations (10) and (11) is 1.7 k. Ω. Hence, the actual fault current, I_{f1}, which will pass into the isolated earth equals 230.4 A.

Figures 5 (a) and (b) show the 3-D dimensions contours of the calculated current density and the electric potential on the earth's surface around the faulty point in the case of

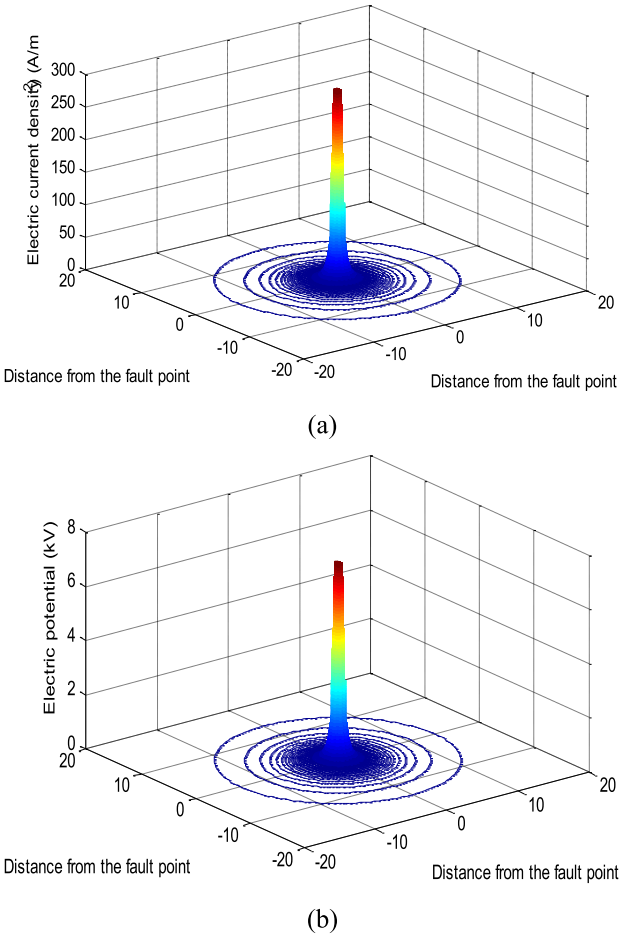

FIGURE 5. Contour of the (a) current density and (b) the electric potential on the earth's surface around the faulty point in case of the isolated system.

homogeneous soil, which are calculated by using equations (13) and (14), respectively. It is noticed that the current density as well as the electric potential have high values near the point of the earth fault, and they decay with the increase of the distance far away from the faulty conductor point. Table 1 presents the influence of the soil resistivity on the touch and step voltages and the current density on the earth's surface, in the case of an isolated system. As it is noticed decreasing the soil resistivity results in a high reduction of step and touch potentials while the current density is maintained approximately constant. In the case of two-layer soils, the reflection factor slightly affects the value of the surface current I_1, as shown in Table 2. The results illustrated in this table are obtained with the assumption that the thickness of the first layer equals 20 m. Also, the contour of the current density on the earth's surface as well as the contour of the electric potential can be calculated and presented.

The influence of the soil resistivity of the second layer on the maximum value of both the touch and step voltages and on the current density at the earth's surface is presented in Table 2. From the results of this table, it is found that the

TABLE 1. Maximum values of the touch and step voltages and the current density on the earth's surface, various the soil resistivity, in case of the isolated system.

ρ (Ω.m)	V_{Touch} (kV)	V_{Step} (kV)	J (kA/m^2)
200	29.3278	26.0863	0.2935
100	14.6627	13.0420	0.2934
50	7.3301	6.5199	0.2934

TABLE 2. Effect of the second layer resistivity on the values of the surface current, I_1, the values of the touch and step voltages and the current density at the earth's surface, in case of nonhomogeneous soil.

ρ_1/ρ_2	reflection factor, k	V_{Touch} (kV)	V_{Step} (kV)	J (kA/m^2)	surface current I_1 (kA)
100/60	-0.25	14.4960	12.8938	0.2901	12.36
100/80	-0.11	14.5796	12.9682	0.2918	12.43
100/100	0	14.6627	13.0420	0.2934	12.5
100/120	+0.09	14.7450	13.1153	0.2951	12.57
100/140	+0.17	14.8267	13.1880	0.2967	12.64

soil resistivity of the second layer and hence the reflection factor has slight effects on the increase of the surface current, I_1, both the touch and step voltages, in addition, the surface current density.

B. RESULTS OF GROUNDED SYSTEM

The charge simulation method with image technique [24] has been employed to calculate the electric potential distribution on the earth's surface when the network is grounded by rods or grids. Then the electric current density is calculated according to [10]. The charge simulation method with the image technique has been checked by calculating the electric potential at some points to indicate the errors at these points and hence the accuracy of the calculation method. It has been noticed that the obtained errors are in the range of 0.02% to 0.05 %, which are acceptable values.

Considering homogeneous soil, Figures 6 (a) and (b) show 3-D contours of the calculated electric potential and the current density on the earth's surface around the faulty point for the grounding system containing one rod as given in Figure 3(b). The rod length is considered 3 m and has a 0.05 m radius. The soil resistivity equals 100 Ω.m as well as its relative permittivity equals 10.

Again, from the obtained results it is noticed that the current density as well as the electric potential near the grounding rod have high values near the grounding rod and they are decreased as the distance from the faulty point increases. This is in agreement with the rule that nearly 90% of resistance between the electrode and soil is within a radius of two meters from the electrode/ rod [27].

Figures 7(a) and (b) and Figures 8(a) and (b) show the 3-D contours of the calculated electric potential and the current

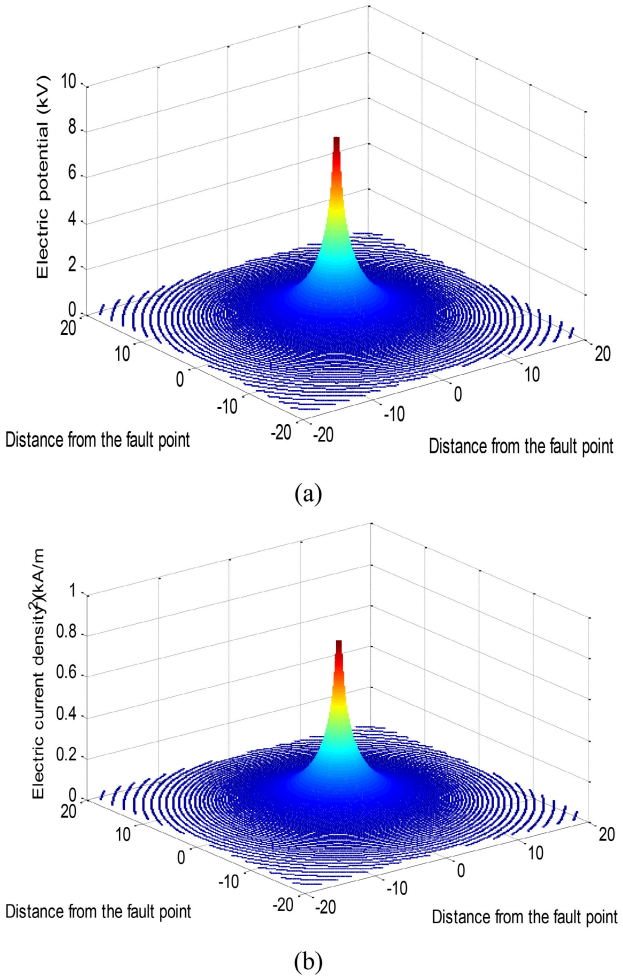

FIGURE 6. Contour of (a) electric potential and (b) the current density on the earth surface around the grounding rod.

density on the earth's surface around three and five grounding rods, used as a grounding system, respectively.

Table 3 shows the impacts of the soil resistivity and number of rods on the maximum values of the touch and step voltages, earth surface current density, and the grounding system resistance. In this table, the distance between any adjacent two rods is considered 4 m, and the soil relative permittivity is taken to be 10. The soil resistivity is taken to be 200, 100, and 50 Ω.m, according to soil types which are sand, clay, and clayey sand, respectively [29]. As noted, the relationships between the soil resistivity with the step and touch voltages, the resistance of the grounding grid, as well as the current density on the soil surface are linear, and these quantities decrease in proportion to the number of rods.

Figure 9 illustrates the effect of the space, S in meters, between two adjacent rods of the grounding grid which contains three and five rods organized in a straight line, on the grounding system resistance, maximum touch and maximum step voltages, and earth surface current density, when the soil resistivity was 50 Ω.m.

TABLE 3. Maximum values of the touch and step voltages, earth surface current density, and the grounding resistance with various numbers of rods, in case of a homogenous soil with different values of soil resistivities.

Number of rods	One rod			Three rods			Five rods		
ρ (Ω.m)	50	100	200	50	100	200	50	100	200
V_{Touch} (kV)	11.30	22.6142	45.2285	0.9297	1.8594	3.7188	0.6069	1.2138	2.4276
V_{Step} (kV)	8.364	16.7297	33.4594	0.5730	1.1460	2.2920	0.3388	0.6776	1.3553
J (kA/m^2)	1.236	1.2363	1.2363	0.1881	0.1881	0.1881	0.1366	0.1366	0.1366
R (Ω)	11.58	23.1757	46.3514	1.2111	2.4221	4.8442	0.8900	1.7800	3.5601

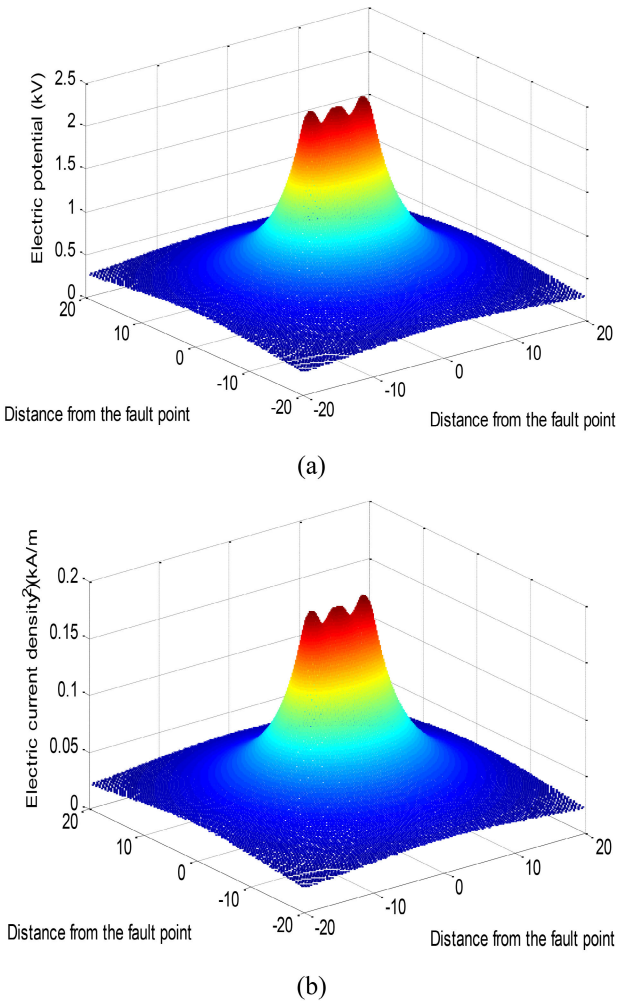

FIGURE 7. Contour of (a) electric potential and (b) the current density on the earth surface around the three grounding rods.

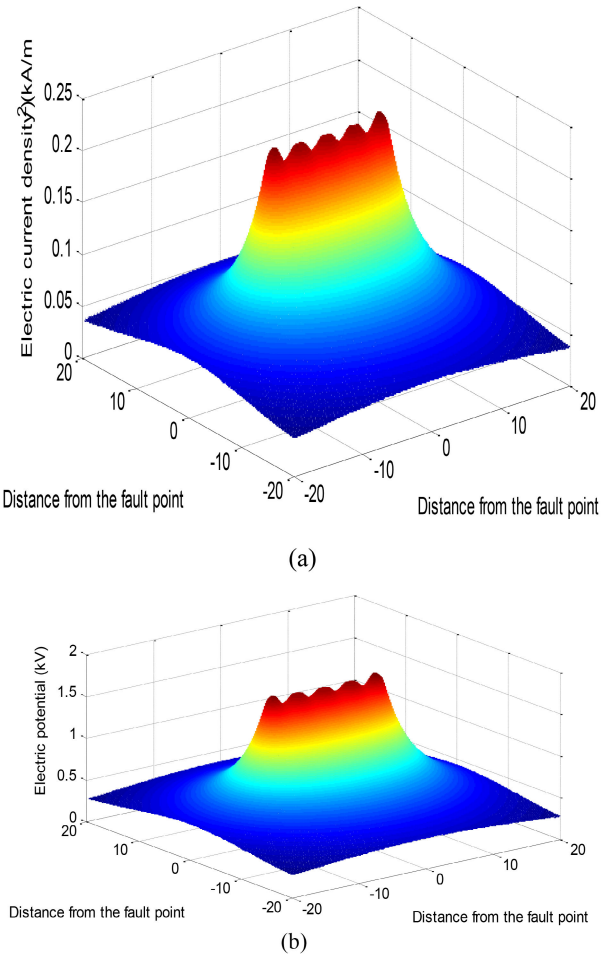

FIGURE 8. Contour of (a) current density on the earth's surface around five grounding rods and (b) electric potential.

From the results of Figure 9, it is noticed that as the space between adjacent two rods is increased, the values of the grounding resistance, the maximum touch voltage, and current density are decreased. The values of the maximum step voltage have been significantly decreased until four meters of space between adjacent two rods, after that, it becomes almost constant, and its change can be neglected with the increase in the space between each two rods. This can be explained by the role that as the space between adjacent two rods is less than the rod length, the overlap effect of resistance areas between the rods increases.

For two-layer soil, Figure 10 illustrates the influence of the second-layer resistivity on the values of the grounding resistance, maximum touch and maximum step voltages, and earth surface current density, with the soil relative permittivity equals 8 for both two layers and the thickness of the first layer equals 20 m, that for a ground system of one, three, and five rods. It is noticed that as the second layer soil resistivity increases, the values of the resistance, the maximum touch and step voltages, and current density are decreased. It should

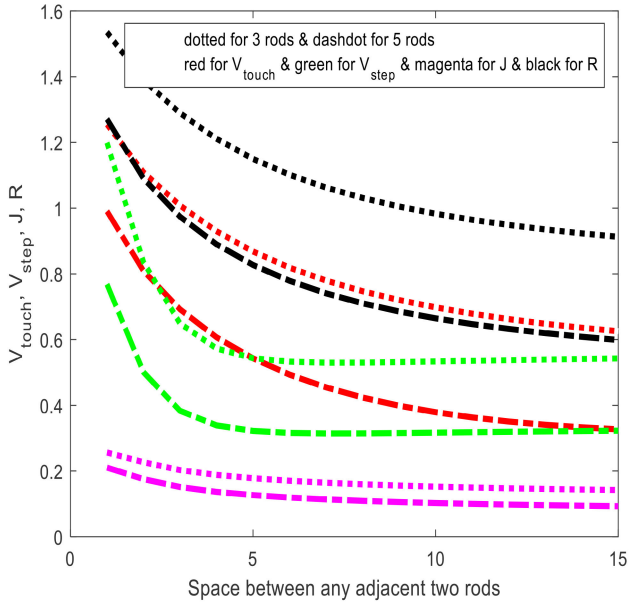

FIGURE 9. Effect of the space between any adjacent two rods of a ground system of three and five rods in meters, on the values of the grounding resistance in ohms, maximum touch and maximum step voltages in kV, and surface current density in kA/m^2, with 50 Ω.m soil resistivity.

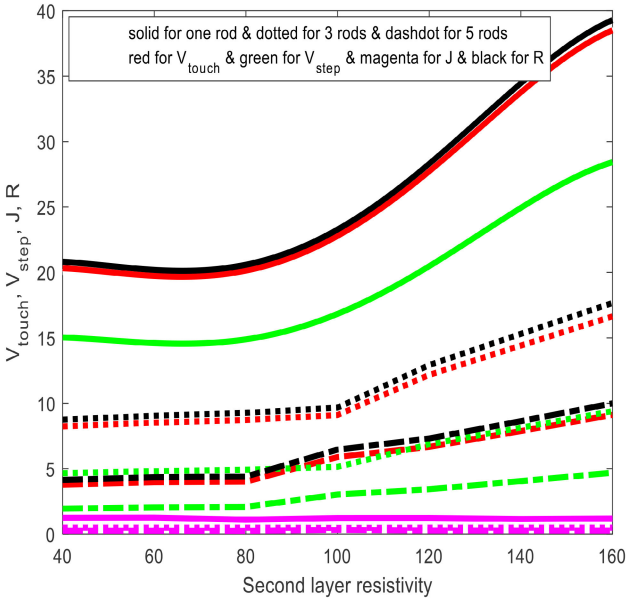

FIGURE 10. Effect of the second layer resistivity in Ω.m on the values of the grounding system resistance in Ω., maximum touch and maximum step voltages in kV and earth surface current density in (kA/m^2), for a ground system of one, three, and five rods.

be noted here that in the case of the grounded system, the change in the soil resistivity has a significant effect compared to the case of the isolated.

The investigated grounding grids have dimensions of 4 m × 4 m with 2 × 2, 4 × 4, 6 × 6 meshes, 0.005 m conductor radius, and the buried depth is considered 0.5 m. The soil resistivity equals 100 Ω.m and its relative permittivity is 10.

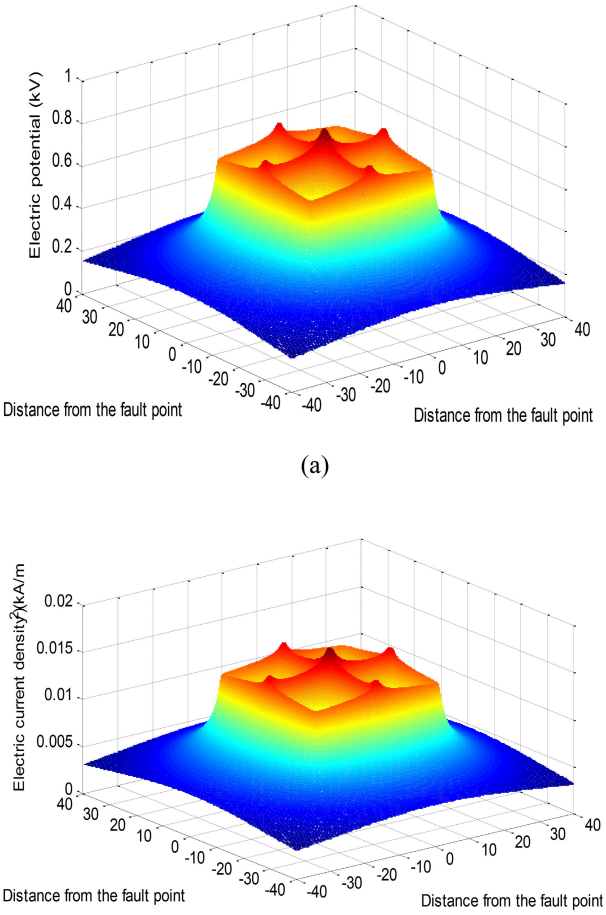

FIGURE 11. Contour of (a) electric potential and (b) the current density on the earth surface around 2 × 2 meshes grounding grid.

The contact resistance of the surrounding earth to the grid is ignored. Considering uniform soil, Figures 11(a) and (b) show the contours of the calculated potential and the current density on the earth's surface for the system containing a grounding grid of 2 × 2 meshes. Figures 12(a) and (b), and Figures 13(a) and (b) show similar results for grounding systems, which contain grids of 4 × 4 and 6 × 6 meshes, respectively.

From the obtained results, it is noticed that the current density as well as the electric potential have a high value at points on the earth surface exactly over the grounding grid, and they decay as the distances of these points on the earth surface from the location of the grounding grid increase.

Figure 14 shows the effect of the homogenous soil resistivity on the values of the grounding resistance, maximum touch and step voltages, and earth surface current density, for grounding grids, which contain 2 × 2, 4 × 4, 6 × 6 meshes, and the grids are buried at 0.5 m depth.

From the tabulated results, it is noticed that as the soil resistivity increases the values of the ground system resistance, maximum touch, and maximum step voltages are increased,

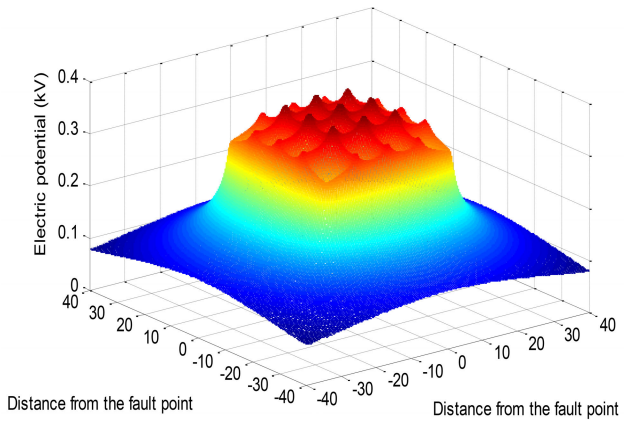

(a)

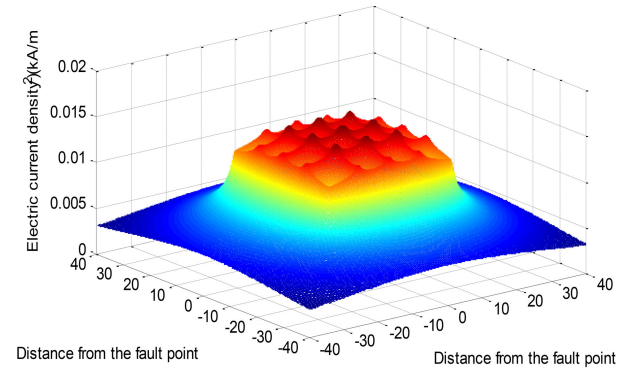

(b)

FIGURE 12. Contour of (a) electric potential and (b) the current density on the earth surface around 4 × 4 meshes grounding grid.

while the values of earth surface current density are constant for each ground grid. That is because as the soil resistivity increases leading to a decrease in the soil conductivity, the ground resistance is increased and the ground surface potential distribution is also increased, hence the product of the gradient of the ground surface potential (electric field) by the soil conductivity is always constant, as the electric field increases by the same rate of decreasing the soil conductivity.

Table 4 shows the effect of the grid depth on the values of the grounding resistance, maximum touch and step voltages, and earth surface current density, for grounding grids of 2×2, 4×4, and 6×6 meshes in a homogenous soil of resistivity equals 100 Ω.m.

From the obtained results of Table 4, it is noticed that, as the laying depths of the grids in a homogenous soil increase, the values of the grounding resistance, maximum touch and step voltages, and earth surface current density are decreased.

Figure 15 shows the impact of the second layer resistivity on the values of the grounding resistance, maximum touch and step voltages and earth surface current density, for grounding grids, which contain 2×2, 4×4, and 6×6 meshes, the grids are buried at laying depth of 0.5m, the thickness of the first layer is considered as 20 m, and the relative permittivity of both two layers is taken as 10.

It is worth mentioning here that the results obtained in this article are in agreement with those obtained in previous studies presented in references [14], [15], [30], and [31].

In order to represent the transient performance model of those vertical grounding electrodes, a transmission line method (TLM) supported with the ATP programme [15] can be utilized to estimate the grounding impedance when injection the lightning current into the vertical grounding electrodes of the tower guidance system. Furthermore, any grounding electrode in the TLM approach may be separated into components, each of which has grounding resistance, capacitance, and inductance as illustrated in Fig. 1(a).

Figure 15 shows the impact of the second layer resistivity on the values of the grounding resistance, maximum touch and step voltages, and earth surface current density, for grounding grids, which contain 2×2, 4×4, and 6×6 meshes, the grids are buried at laying depth of 0.5 m, the thickness of the first layer is considered 20 m as an example of the calculations, and the relative permittivity of both two layers is taken as 10.

Table 5 gives a comparison between the results obtained in this article and the results of previous studies by calculating the difference with the proposed methodology.

V. EXPERIMENTAL MODELS FOR THE VALIDATION OF THE CALCULATED RESULTS

In this section, the validation of the calculated results is performed by comparing some of the calculations with the measurements carried out by the use of experimental models.

Figure 16(a) obvious the components of the experimental setup, which contains, a glass electrolytic tank that has dimensions of 1 m × 1 m × 0.5 m. The tank's inner surface is covered by a conducting metallic sheath. Moreover, tap water is utilized as an electrolyte, representing homogenous soil. Hence, its electric resistivity equals 33.4 Ω.m. Note that the electrolytic resistivity can be controlled by modifying the salinity of the tap water by adding a specific amount of Sodium Chloride salt. Further, the applied voltage to the grid is under control by an auto-transformer until the value of current reaches 1 A with a scaling factor 1: 1000 of short circuit current tends to 1 kA. In addition, a voltmeter is employed to measure the output voltage from the auto-transformer and applied to the grounding grid model (V_s).

Another voltmeter is applied also to measure the surface potential (V_m) through the diagonal of the grounding system in these tests. Furthermore, an ammeter is utilized to measure the current that follows within the electrolyte between the return earthed electrode and the model grid. The scale factor of 20:1 for the tested grids with outside dimensions of 20 cm × 20 cm has been modeled and tested to be compared with calculations, which are carried out by the same data. Note that the diameter of simulated grid conductors is 2.5 mm and made from copper.

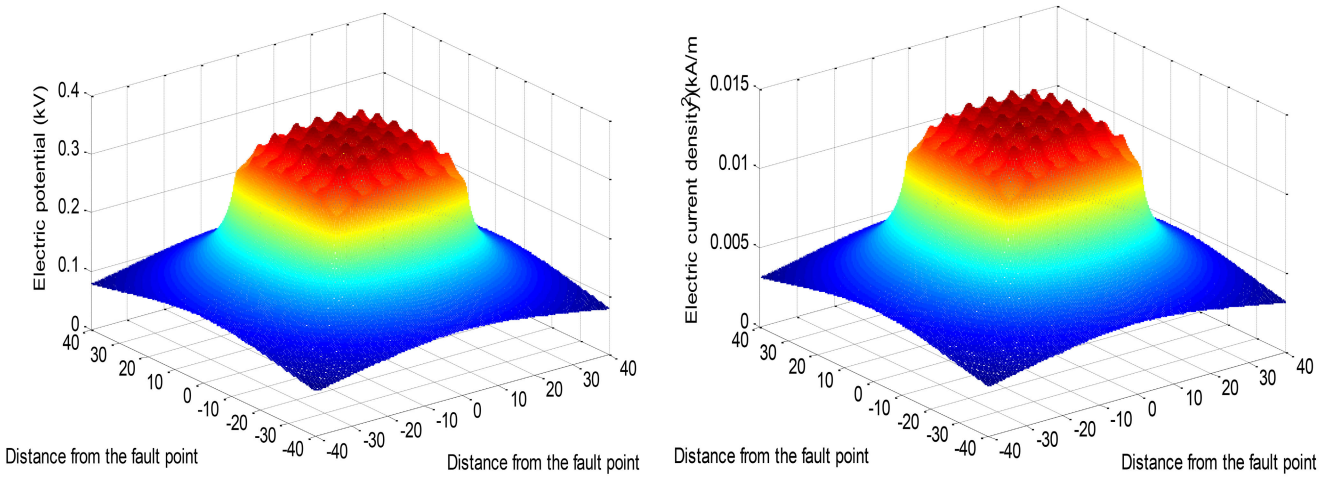

FIGURE 13. Contour of (a) electric potential and (b) the current density on the earth surface around 6 × 6 meshes grounding grid.

TABLE 4. Effect of the grid depth on the values of the ground system resistance, maximum touch and maximum step voltages, and earth surface current density, for grounding grids of 2 × 2, 4 × 4, and 6 × 6 meshes in a homogenous soil.

Grid	2×2			4×4			6×6		
d (m)	0.5	1	1.5	0.5	1	1.5	0.5	1	1.5
V_{Touch} (kV)	1.8243	1.4783	1.4422	1.3108	1.2690	1.2401	1.2299	1.1939	1.1672
V_{Step} (kV)	0.0301	0.0981	0.0671	0.1337	0.0788	0.0559	0.1162	0.0709	0.0520
J(kA/m^2)	0.1728	0.0278	0.0262	0.0275	0.0260	0.0250	0.0266	0.0255	0.0247
R(Ω)	1.5359	1.7667	1.7306	1.5982	1.5563	1.5274	1.5170	1.4809	1.4541

Figure 16(b) illustrates the experimental model to simulate two-layer soils. Two matching tanks; each one having dimensions 1 m × 1 m × 0.5 m, filled with tap water. One tank is positioned on top of the other, and the lower tank's top end has a plastic coating to create electrical isolation between their metallic bodies. Where the electrical contact between two mediums (means two layers soil) happens through the metallic base of the upper tank. Hence, the bottom tank is linked to the earth. The water resistivity of each tank is altered by adding an sufficient amount of salt. The resistivity of the water is measured by means of a DC probe. The measured values were 9.94 Ω.m and 25 Ω.m for the upper tank and lower tanks, respectively. The height of the water in the upper tank was 5 cm. Note that the water model temperature is 26 °C for the two layers soil throughout voltage profile measurements.

The parameters of the vertical rod used in these experimental tests are as follows: the vertical electrode length was 3 cm, and its radius was 0.5 mm. The thickness of the first layer, in the nonhomogeneous experimental model was 5 cm. Fig. 17(a) illustrates a comparison between the calculated earth surface potential by the present approach and the experimental earth surface potential in homogenous water for the vertical grounding rod.

Figure 17(b) shows similar results in the two-layer soil simulated by water layers for the vertical grounding rod. It is seen that the measured values are a little bit changed compared with the estimated values, where the reason behind that is due to the boundary effects of the tank walls. In general, it is noticed that the experimental results give good agreement with the simulated results.

Figure 17(c) illustrates a comparison between the experimental results and the present method results of a square ground grid of (2 × 2) four meshes. It is observed that there is a good agreement between the obtained results from both two methods. Fig. 17(d) shows the earth surface potential of the proposed algorithm and experimental potential along the diagonal of the square grounding grids of (2 × 2) four meshes.

It is obvious that the measured values give good agreement with simulated results.

To simulate the isolated system the connection of the tank of each model with earth is removed and the measurements are carried out by the use of the same data and the current density is measured using current density probe Model

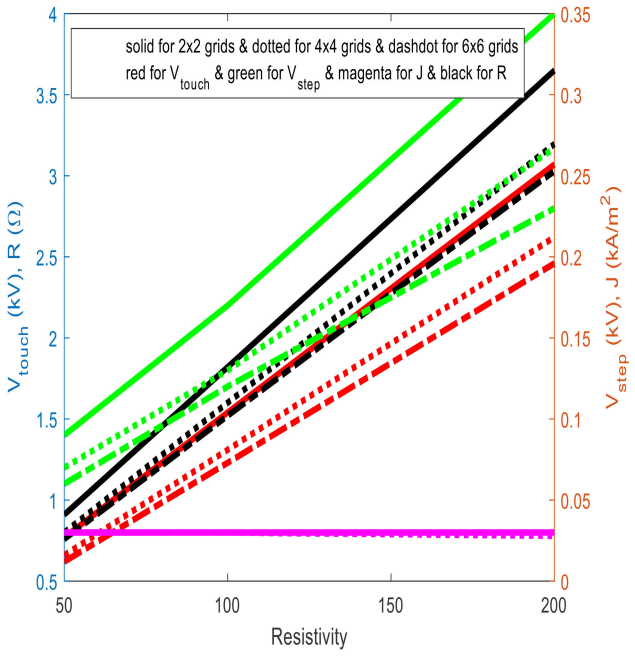

FIGURE 14. Influence of the soil resistivity in Ω.m on the values of the grounding resistance in Ω, maximum touch and step voltages in kV, and earth surface current density in (kA/ m^2), for grounding grids of 2 × 2, 4 × 4, and 6 × 6 meshes.

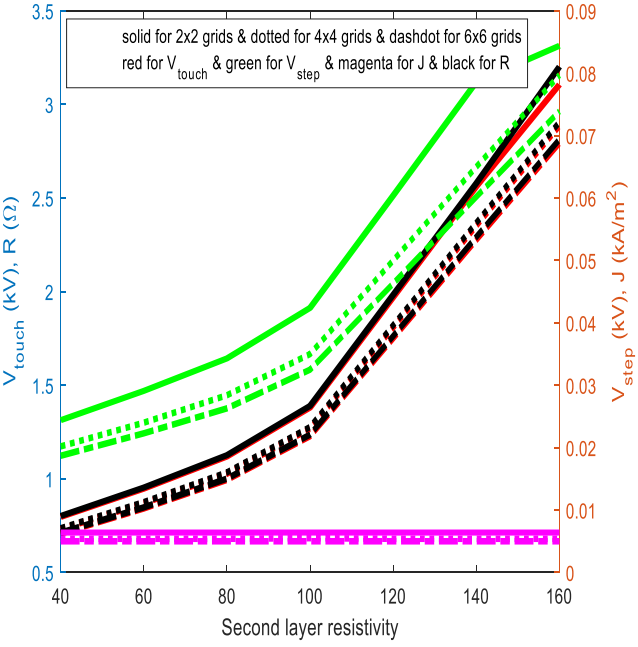

FIGURE 15. Effect of the second layer resistivity on the values of the ground system resistance, maximum touch and maximum step voltages, and earth surface current density, for a ground system of 2 × 2, 4 × 4, and 6 × 6 grids, where the grids are buried at depth equals 0.5 m. r = 0.02 m.

AC-10. The results are illustrated in Table 6. Good agreement is observed.

VI. COMPARISON BETWEEN ISOLATED AND GROUNDED SYSTEMS

Table 7 shows examples of the calculated results of the current density, and maximum touch and step voltages for isolated and grounded systems. From this table, it is clear that the grounding system reduces the Ground Potential Rise (GPR) and hence the current density by significant values. Also, it is clear that the grounding by using grids has a great effect in reducing the GPR compared with the use of rods.

From Table 7, it is noticed that the grounding system compared with the isolated system has reduced the touch potential by about 10.6 and 11.9 times, the step voltage by 17 and 112 times, and the current density is lowered by 1.937 and 11.03 times in the case of using grounding rods and grounding grids, respectively.

From the aforementioned values, it is concluded that the grounding system of electric power stations, transmission,

TABLE 5. Comparison between the results obtained in this article and the results of previous studies.

Investigated case by the present approach	Investigated cases by the other approaches	Difference %
The calculated ground potential rise is 29.3278 kV per each 1 kA	the ground potential rise calculated by references [14, 15] is 30 kV per each 1 kA at the Sara substation.	2.2 %
The current density was .0266 (kA/m^2).	The current density by references [14, 15] was 0.03 (kA/m^2).	2.46 %
The step and touch voltages are calculated in cases of uniform and double-layer soils.	There is harmony with the results reported by ref. [30] in the case of the equal space grounding grids, regardless of the fault current and the soil resistivity values, as well as the dimensions of the grounding grids.	There is harmony between the obtained results and that reported by ref. [30].
The actual fault current I_{fi}, which will pass into the isolated earth equals 230.4 A.	Earth fault current at similar conditions used in the calculations in the present approach is 231.64 A [31].	0.5 %

TABLE 6. Current density, touch, and step voltages for isolated and grounded systems.

Cases	V_{Touch} (kV)	V_{Step} (kV)	J (kA/m^2)
Calculated Isolated system	0.73	0.659	0.0231
Measured values	0.7	0.6833	0.022

TABLE 7. Current density, touch, and step voltages for isolated and grounded systems.

Cases	V_{Touch} (kV)	V_{Step} (kV)	J (kA/m^2)
Isolated earth	7.3301	6.5199	0.2934
Grounding rod (five rods)	0.6920	0.3833	0.1515
Grounding grid (6×6)	0.6150	0.0581	0.0266

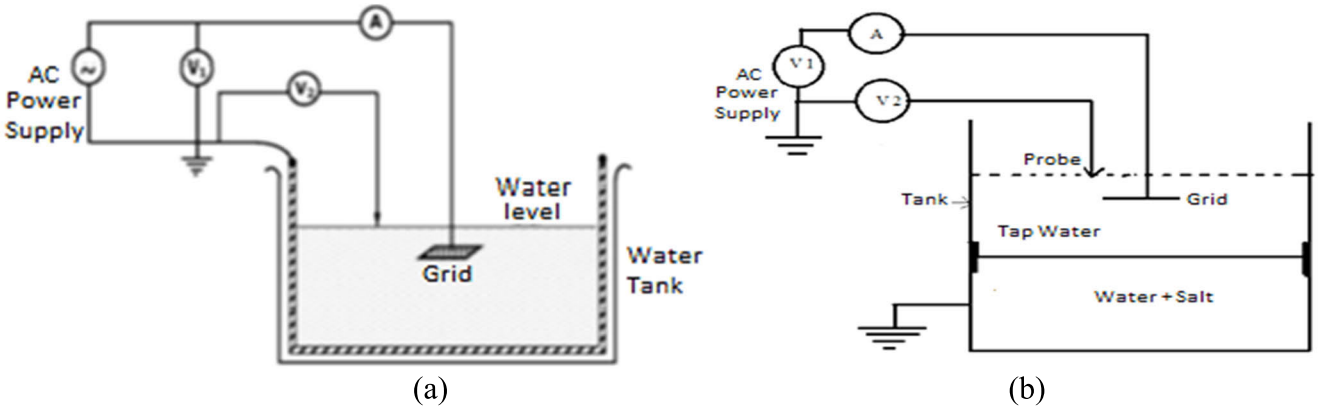

FIGURE 16. Experimental setup, (a) Homogenous soil model and (b) Model of two layers soil.

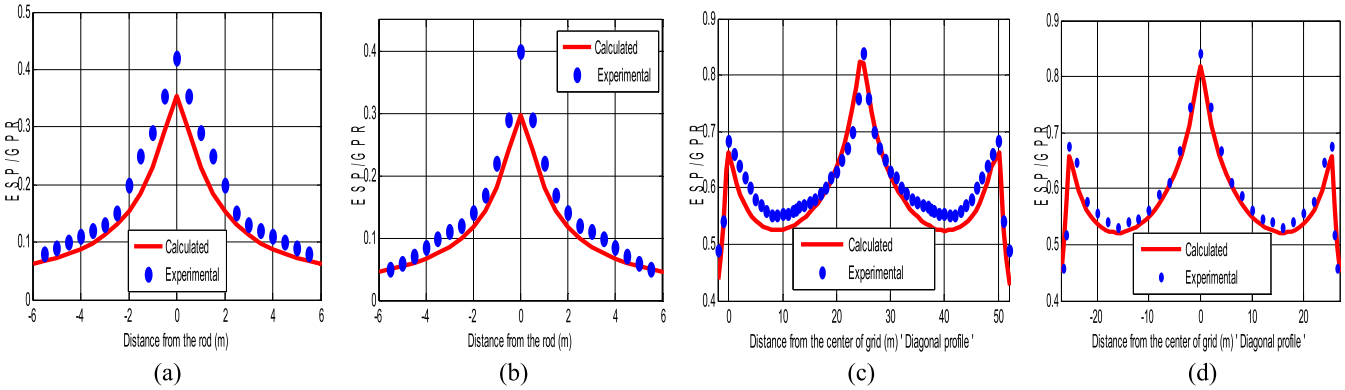

FIGURE 17. Earth surface potential comparison of (a) grounding rod in a homogenous soil, (b) vertical grounding rod in a nonhomogeneous soil, (c) 4 meshes square grounding grid in a homogenous soil, and (d) 4 meshes square grounding grid in a nonhomogeneous soil.

and distribution lines represents an important protection for workers in the sites and for human activities in the areas surrounding their locations. From the obtained results, in previous sections, it is noticed that the soil resistivity affects greatly the potential distribution on the earth's surface. It is noticed also that the potential distribution values decrease as the soil resistivity decreases. On the other hand, for each case under study, the soil resistivity has no influence on the values of the current density distribution on the earth surface. This can be understood as the change in the value of the soil resistivity is accompanied by a change in the resistance of the earth's surface and, accordingly, a change in the earth's potential rise, which results in stability in the value of the current density.

VII. CONCLUSION

In this article, a novel approach for calculating the current density and the grounding potential raised on the earth's surface due to line-to-ground fault current with and without a grounding system has been introduced. Two cases were considered under study, namely: isolated earth and with the presence of the grounding system (grounding rod and grounding grid). The proposed approach enjoys ease of application and simplicity. It does not need complex computer programs or a long time for calculations. It has a high accuracy of the results obtained by its applications in the cases of isolated and grounded electrical networks.

From the obtained results it is noticed that the current density as well as the grounding potential rise have high values at points on the earth's surface near to the earth's fault point, and they decay as the distances of these points on the earth's surface from the fault point increase. Also, it is proved that the ground system reduces the Ground Potential Rise and hence the current density by a significant value. Finally, for each case under study, it is noticed that the value of the soil resistivity has a significant effect on the potential distribution on the earth's surface and has no effect on the values of the current density distribution on the earth surface. Experimental models for the validation of the calculated results are presented in good agreement with the proposed approach.

As an extension of this research, it is recommended in the future to devise a similar model to investigate the influences of lightning strokes on isolated and grounded networks. Application of the proposed on multi-layer soils is recommended for future work.

ACKNOWLEDGMENT

This work was supported by the Department of Electrical Engineering and Automation, School of Electrical Engineering, Aalto University, Espoo, Finland.

REFERENCES

[1] J. He, B. Zhang, and R. Zeng, "Maximum limit of allowable ground potential rise of substation grounding system," *IEEE Trans. Ind. Appl.*, vol. 51, no. 6, pp. 5010–5016, Nov. 2015.

[2] M. B. Bastian, W. D. Carman, and D. J. Woodhouse, "Real-time monitoring of substation ground potential rise and grounding system impedance using power system faults," *IEEE Trans. Ind. Appl.*, vol. 51, no. 6, pp. 5298–5304, Nov. 2015.

[3] C.-N. Chang and C.-H. Lee, "Computation of ground resistances and assessment of ground grid safety at 161/23.9-kV indoor-type substation," *IEEE Trans. Power Del.*, vol. 21, no. 3, pp. 1250–1260, Jul. 2006.

[4] N. Nichols and D. D. Shipp, "Designing to avoid hazardous transferred Earth potentials," *IEEE Trans. Ind. Appl.*, vol. IA-18, no. 4, pp. 340–347, Jul./Aug. 1982.

[5] R. A. Harvie, "Hazards during ground faults on 480-V grounded systems," *IEEE Trans. Ind. Appl.*, vol. IA-10, no. 2, pp. 190–196, Mar. 1974.

[6] G. Parise, L. Parise, and L. Martirano, "The interference of grounding systems: The floating behavior," *IEEE Trans. Ind. Appl.*, vol. 51, no. 6, pp. 5038–5043, Nov./Dec. 2015.

[7] B. Zhang, Y. Jiang, J. Wu, and J. He, "Influence of potential difference within large grounding grid on fault current division factor," *IEEE Trans. Power Del.*, vol. 29, no. 4, pp. 1752–1759, Aug. 2014.

[8] F. Dawalibi and D. Mukhedkar, "Parametric analysis of grounding grids," *IEEE Trans. Power App. Syst.*, vol. PAS-98, no. 5, pp. 1659–1668, Sep. 1979.

[9] C.-H. Lee and C.-N. Chang, "Comparison of 161/69-kV grounding grid design between indoor-type and outdoor-type substations," *IEEE Trans. Power Del.*, vol. 20, no. 2, pp. 1385–1393, Apr. 2005.

[10] Z.-X. Li, Y. Yin, C.-X. Zhang, and L.-C. Zhang, "Numerical simulation of currents distribution along grounding grid buried in horizontal multi-layered Earth in frequency domain based dynamic state complex image method," *Electr. Power Compon. Syst.*, vol. 43, no. 14, pp. 1573–1582, Aug. 2015.

[11] H. M. E. Misilmani, K. Y. Kabalan, M. Y. Abou-Shahine, and M. Al-Husseini, "A method of moment approach in solving boundary value problems," *J. Electromagn. Anal. Appl.*, vol. 7, no. 3, pp. 61–65, 2015.

[12] R. Alipio, M. A. O. Schroeder, and M. M. Afonso, "Voltage distribution along Earth grounding grids subjected to lightning currents," *IEEE Trans. Ind. Appl.*, vol. 51, no. 6, pp. 4912–4916, Nov. 2015.

[13] O. E. Gouda, A. Z. E. D. Mohamed, M. M. Al-Harthi, S. Y. Omar, and S. S. M. Ghoneim, "Performance of grounding electrodes under lightning strokes in uniform and two-layer soils considering soil ionization," *IEEE Access*, vol. 10, pp. 76855–76869, 2022.

[14] P. Colella, R. Napoli, E. Pons, R. Tommasini, A. Barresi, G. Cafaro, A. De Simone, M. L. Di Silvestre, L. Martirano, P. Montegiglio, E. Morozova, G. Parise, L. Parise, E. R. Sanseverino, F. Torelli, F. Tummolillo, G. Valtorta, and G. Zizzo, "Current and voltage behaviour during a fault in a HV/MV system: Methods and measurements," in *Proc. IEEE 15th Int. Conf. Environ. Elect. Eng. (EEEIC)*, Rome, Italy, Jun. 2015, pp. 404–409.

[15] E. Pons, P. Colella, R. Napoli, and R. Tommasini, "Impact of MV ground fault current distribution on global earthing systems," *IEEE Trans. Ind. Appl.*, vol. 51, no. 6, pp. 4961–4968, Nov. 2015.

[16] L. Boyer, "Contact resistance calculations: Generalizations of Greenwood's formula including interface films," *IEEE Trans. Compon. Packag. Technol.*, vol. 24, no. 1, pp. 50–58, Mar. 2001.

[17] R. S. Timsit, "Constriction resistance of thin film contacts," *IEEE Trans. Compon. Packag. Technol.*, vol. 33, no. 3, pp. 636–642, Sep. 2010.

[18] R. Holm, *Electric Contacts: Theory and Application*, 4th ed. Berlin, Germany: Springer-Verlag, 1967.

[19] W. Tang, M. R. Gomez, Y. Y. Lau, R. M. Gilgenbach, and J. Zier, "Theory and experimental measurements of contact resistance," in *Proc. IEEE Int. Conf. Plasma Sci.*, San Diego, CA, USA, Jun. 2009, pp. 1–5.

[20] S. Sawada, K. Shimizu, Y. Hattori, T. Tamai, and K. Iida, "Analysis of contact resistance behavior for electric contacts with plating layer," in *Proc. 56th IEEE Holm Conf. Electr. Contacts*, Charleston, SC, USA, Oct. 2010, pp. 1–8.

[21] P. Zhang and Y. Y. Lau, "Constriction resistance and current crowding in vertical thin film contact," *IEEE J. Electron Devices Soc.*, vol. 1, no. 3, pp. 83–90, Mar. 2013.

[22] V. V. Terzija and H.-J. Koglin, "On the modeling of long arc in still air and arc resistance calculation," *IEEE Trans. Power Del.*, vol. 19, no. 3, pp. 1012–1017, Jul. 2004.

[23] V. V. Terzija, R. Ciric, and H. Nouri, "Improved fault analysis method based on a new arc resistance formula," *IEEE Trans. Power Del.*, vol. 26, no. 1, pp. 120–126, Jan. 2011.

[24] E. Bendito, A. Carmona, A. M. Encinas, and M. J. Jiménez, "The extremal charges method in grounding grid design," *IEEE Trans. Power Del.*, vol. 19, no. 1, pp. 118–123, Jan. 2004.

[25] V. V. Terzija, R. M. Ciric, and H. Nouri, "A new iterative method for fault currents calculation which models arc resistance at the fault location," *Electr. Eng.*, vol. 89, no. 2, pp. 157–165, Dec. 2006.

[26] O. E. Gouda, T. El-Saied, W. A. A. Salem, and A. M. A. Khater, "Evaluations of the apparent soil resistivity and the reflection factor effects on the grounding grid performance in three-layer soils," *IET Sci., Meas. Technol.*, vol. 13, no. 4, pp. 572–581, Jun. 2019.

[27] *IEEE Guide for Safety in AC Substation Grounding*, IEEE Standard (80-2013) (Revision of IEEE Standard 80-2000/Incorporates IEEE Standard 80-2013/Cor 1-2015), Institute of Electrical and Electronics Engineers, New York, NY, USA, May 2015, pp. 1–226.

[28] J. A. Sullivan, "Alternative earthing calculations for grids and rods," *IEE Proc., Transmiss. Distrib.*, vol. 145, no. 3, pp. 271–280, 1998.

[29] J. M. Reynolds, *An Introduction to Applied and Environmental*. New York, NY, USA: Wiley, 1997. [Online]. Available: https://www.academia.edu/35804474/An_Introduction_to_Appliedand_Environmental_Geophysics

[30] O. E. Gouda and A. Z. E. Dein, "Ground potential rise of faulty substations having equal and unequal spacing grounding grids conductors," *IET Gener., Transmiss. Distrib.*, vol. 11, no. 1, pp. 18-26, Jan. 2017.

[31] A. L. Fredriksen, "Earth fault protection in isolated and compensated power distribution systems," M.S. thesis, Master Energy Environ. Eng., Dept. Elect. Power Eng., Norwegian Univ. Sci. Technol., Trondheim, Norway, Jun. 2016. Accessed: Mar. 30, 2022. [Online]. Available: https://ntnuopen.ntnu.no/ntnu-xmlui/handle/11250/2402539

OSAMA E. GOUDA was born in 1951. He received the B.Sc. degree in electrical engineering and the M.Sc. and Ph.D. degrees in high voltage from Cairo University, Egypt, in 1975, 1979, and 1982, respectively. From 1988 to 1993, he was an Associate Professor with the Department of Electrical Power Engineering, Faculty of Engineering, Cairo University. In 1988, he was with the Department of Electrical Engineering, Kema Institute, Arnhem, The Netherlands, where he was a Research Fellow. Since 1993, he has been a Full Professor with the Electrical Engineering Department, Cairo University, where he is currently the Head of the High Voltage Group, Electrical Power Engineering Department. He has published more than 140 papers. He was the supervisor for about 70 M.Sc. and Ph.D. degrees. His research interests include high-voltage phenomena, cable insulation, protection of power systems, and electromagnetic transients. He is a Regular Reviewer of many IEEE TRANSACTIONS, *IET Generation, Transmission and Distribution*, and *Electric Power Systems Research*.

ADEL Z. EL DEIN was born in Egypt, in 1971. He received the B.Sc. and M.Sc. degrees in electric engineering from the Faculty of Energy Engineering, Aswan, Egypt, in 1995 and 2000, respectively, the Ph.D. degree in electric engineering from Kazan State Technical University, Kazan, Russia, in 2005, and the Doctor of Engineering degree from Kazan State Technical University. From 1997 to 2002, he was a Teaching Assistant with the Faculty of Energy Engineering, Aswan, Egypt. From 2002 to 2005, he was with the Kazan Energy Institute, Kazan, and with Kazan State Technical University. From 2005 to 2011, he was a Staff Member with the Department of High Voltage Networks, Faculty of Energy Engineering, Aswan University, Aswan, where he was an Associate Professor, from 2011 to 2016. In 2014, he joined the Department of High Voltage Engineering (Hikita Laboratory), Kyushu Institute of Technology (KIT), Japan, as a Researcher. Since 2016, he has been a Full Professor of high voltage engineering with the Department of High Voltage Networks, Faculty of Energy Engineering, Aswan University. In October 2022, he became the President of New Thebes Technological University, Luxor, Egypt. His research interests include the calculation of electric and magnetic fields and their effects and the comparison of numerical techniques in electromagnetics. He is a Regular Reviewer of IEEE TRANSACTIONS ON POWER DELIVERY, *Electric Power Systems Research*, and *IET Generation, Transmission and Distribution*.

ELSAYED TAG-ELDIN is currently with the Faculty of Engineering and Technology, Future University in Egypt, on leave from Cairo University, Egypt, after nearly 30 years of service to the Faculty of Engineering. He was the Dean of the Faculty of Engineering, Cairo University, where he achieved many unique signs of progress in both academia and research on the impact of emerging technologies in electrical engineering. Also, he was a PI of several nationally and internationally funded projects. He has many publications in highly refereed international journals and specialized conferences on the applications of artificial intelligence in the protection of electrical power networks. His research interests include the calculation of electric and magnetic fields and their effects and the comparison of numerical techniques in electromagnetics. He is on the editorial boards and a reviewer of several international journals.

MATTI LEHTONEN received the master's and Licentiate degrees in electrical engineering from the Helsinki University of Technology, Finland, in 1984 and 1989, respectively, and the Doctor of Technology degree from the Tampere University of Technology, Finland, in 1992. He was with VTT Energy, Espoo, Finland, from 1987 to 2003. Since 1999, he has been a Full Professor and the Head of the Power Systems and High Voltage Engineering Group, Aalto University, Espoo. His research interests include power system planning and assets management, power system protection, including earth fault problems, harmonic related issues, high voltage systems, power cable insulation, and polymer nanocomposites. He is an Editor and a Special Issue Editor of *IET Generation, Transmission and Distribution* and an Associate Editor of *Electric Power Systems Research*.

MOHAMED M. F. DARWISH (Senior Member, IEEE) was born in Cairo, Egypt. He received the B.Sc., M.Sc., and Ph.D. degrees in electrical engineering from the Faculty of Engineering at Shoubra, Benha University, Cairo, in May 2011, June 2014, and January 2018, respectively. From 2016 to 2017, he was a Ph.D. Student with the Department of Electrical Engineering and Automation (EEA), Aalto University, Finland, under Prof. M. Lehtonen's Group. Since January 2023, he has been an Associate Professor with the Department of Electrical Engineering, Faculty of Engineering at Shoubra. He was also a Postdoctoral Researcher with the Department of EEA, School of Electrical Engineering, Aalto University. He has coauthored several international IEEE journals and conferences. His research interests include high voltage, cable insulation, fault diagnosis, polymer nanocomposites, nano-fluids, partial discharge, DGA, renewables, applied machine learning, the IoT, and industry 4.0. He received the Best Ph.D. Thesis Prize that serves industrial life and society all over the Benha University Staff for the academic year, from 2018 to 2019. From 2021 to 2022, he received the Benha University Encouragement Award in the field of engineering sciences and technology. Since 2021, he has been a Topic Editor of *Catalysts* (MDPI), also becomes a guest editor of several special issues. In 2022, he was nominated as a Young Editorial Board Member of *Applied Energy*. He was a Subject Editor and an Associate Editor of *IET Generation, Transmission and Distribution* and *Frontiers in Energy Research*. In addition, he was an Editor of the *Electric Power Components and Systems*. In 2023, he was promoted to an Associate Editor of *High Voltage*.